

# Extending Persistent Monitoring by Combining Ocean Models and Markov Decision Processes

Wesam H. Al-Sabban, Luis F. Gonzalez and Ryan N. Smith  
School of Electrical Engineering and Computer Science  
Queensland University of Technology, Brisbane, QLD, Australia  
Corresponding author email: ryan.smith@qut.edu.au

**Abstract**—Ocean processes are complex and have a high variability in both time and space. Thus, ocean scientists must collect data over long time periods to obtain synoptic views and resolve multidimensional spatiotemporal variability. In this paper, we present a methodology for incorporating time-varying currents into a Markov Decision Process for persistent path execution by underwater gliders. The application of an hybrid Gaussian distribution of ocean currents and a modified Markov Decision Process technique enables the incorporation of uncertainty from a deterministic ocean model. The proposed approach achieves improved navigational accuracy, and can extend the distance travelled over the duration of a mission. We present a derivation of our methodology, an outline of the proposed algorithms, and simulation predictions that are validated through experimental field trials.

## I. INTRODUCTION

Due to the dynamic complexity of many ocean processes, and their high spatiotemporal variability, it is imperative to gather data over long time periods. This implies that in addition to creating an historical time-series data-set, sampling missions must also maintain a persistent presence in the environment. One way to accomplish this is through the use of Autonomous Underwater Vehicles (AUVs) that are able to stay on deployment for long periods, e.g., autonomous gliders [1]. Enabling persistence for aquatic vehicles directly relates to decreasing actuation. Thus, a challenge for persistent ocean monitoring is dealing with ocean currents while executing a mission, as these disturbances can be on the order of the vehicle velocity. Here, we present a mission planning method for persistent monitoring that exploits ocean currents to increase navigational accuracy and extend the possible distance travelled.

In general, a suitable sampling resolution for a given process is not known a priori. In contrast, the general area of study and/or region(s) of interest, and a specific process or feature of interest are clearly identified. This motivates researchers to improve current methodology in the field of planning for autonomous robots [2]. An ocean scientist, with expert domain knowledge, can easily classify locations within a given region that are of greater scientific interest, for that specific process, than other locations. For example, in shelf break regions, the water depth decreases rapidly toward shore. The interaction of physical forcing with the bathymetry and coastline can result in coastal upwelling, diapycnal mixing, and generation of internal tides and waves that may break near the coast,

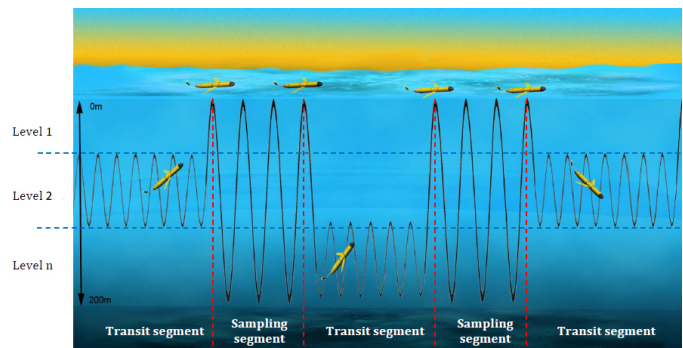


Fig. 1. An example path showing the partitioning between transit segments and sampling segments. Full-depth profiles are performed in sampling regions, while transit regions exploit favourable layers of current.

all of which contribute to upward transport of nutrients in the coastal region, and are of interest for the study of algal bloom formation. Given this motivation, we are interested in developing methods to intelligently sample ocean regions persistently, to aid in the understanding of the spatiotemporal variability of dynamic processes occurring within this region.

Partitioning a region into ranked areas of interest has been demonstrated to provide novel methods for persistent monitoring [3]. Here, we view this partitioning as a way to break-up a predefined sampling path into designated *sampling regions* and *transit regions*, as shown in Fig. 1. Similar to the method proposed in [3], we compute an execution plan that provides dense sampling in the survey regions, and more sparse sampling in the transit regions. Instead of varying the velocity of the vehicle within the regions of lower interest, we propose to target layers of favourable current predicted by an ocean model within the transit regions. In this way, the vehicle achieves a better navigational accuracy, and extends the overall distance travelled for the duration of the mission as demonstrated in [4], [5].

### A. Motivation

The primary region of interest for this study is the Southern California Bight (SCB) (the oceanic region contained within  $32^\circ\text{N}$  to  $34.5^\circ\text{N}$  and  $117^\circ\text{E}$  to  $121^\circ\text{E}$ ). The motivation is to determine physical factors contributing to the formation and evolution of algal blooms within the region. Ongoing study within this area provides a predefined region of interest,

locations of high sampling priority, and a sampling path given by an ocean scientist with expert domain knowledge [6]. The predefined region of interest within the SCB is presented in Fig. 2. The outline of the region of interest is given by the blue line, and the two shaded areas Q1 and Q2 specify the high interest sampling regions. The numbers (1,2,3,4,5,6) identify the main waypoints for mission planning. The dashed line represents the transition portion of each segment, and the red line represents the sampling portion of each segment. The blue circles identify the intersection of each segment with the sampling region. The length of each segment is presented in Table I.

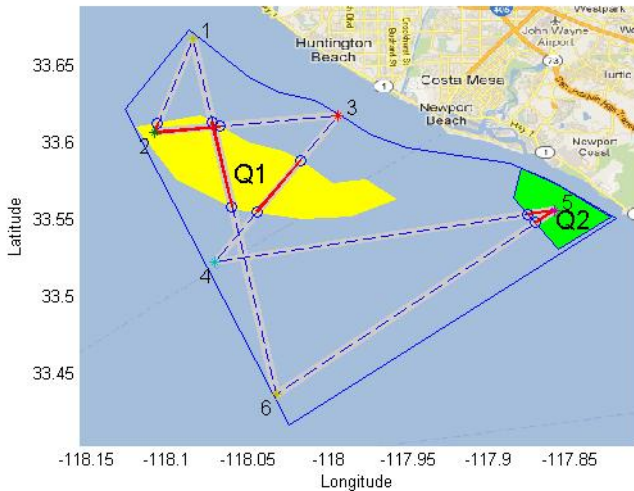


Fig. 2. The blue line identifies the region of interest, with Q1 and Q2 specifying regions of high interest. The numbers (1,2,3,4,5,6) relate to the waypoints for our mission planning. The dashed line shows the transition portions of each segment, and the red line shows the sampling portion of each segment. The blue circle shows the intersection between each segment and the sampling region.

TABLE I  
THE LENGTH OF TRANSITION SEGMENTS AND SAMPLING SEGMENTS IN THE PROJECT AS SHOWN IN FIG. 2

Segment	Transit (km)	Sampling (km)	Total (km)
1-2	6.4774	0.626	7.1034
2-3	6.8962	3.7875	10.6837
3-4	3.969 4.4139	4.4384	12.8213
4-5	18.37	1.55	19.92
5-6	19.43	1.42	20.85
6-1	13.847 6.127	6.182	26.156

## II. BACKGROUND

There have been many studies on planning optimal-information and adaptive paths for environmental monitoring. However none of these methods address the persistence problem in the ocean, while additionally incorporating the unique constraints and abilities of autonomous gliders. Here, we take advantage of this vehicle's persistent, long-term surveillance, and provide missions that can increase navigational accuracy and extend overall distance travelled.

Path planning and execution for AUVs that exploit ocean currents is an active area of research. Multiple approaches using different searching algorithm technique such as Linear Programming [7], [8] probabilistic sampling methods, e.g., Rapidly-Exploring Random Trees (RRTs) or Genetic Algorithms (GAs) [9], and Artificial Intelligence methods, e.g., A\* [10], [11], have been developed and implemented. Specifically, Alvarez and Caiti [12] used dynamic programming to generate an optimal AUV path plan that reduces the on-board energy consumption using the spatial structure of the current velocity field. Results show essential energy saving, as compared to straight line paths. In 2004, Alvarez et al. [13] considered optimizing the energy cost of AUV mission planning in ocean environments with real current fields. The authors assumed the AUV speed with respect to the bottom is constant and the considered AUV was able to change its speed depending on the current field to keep the total speed constant through the planned path. A more common situation where the thrust power of AUV maintained constant through the operation had been considered by Garau et al. [14]. The A\* algorithm was adapted to find the minimum time path will optimize the energy consumption of the AUV. In 2009 Garau et al. [15] applied the proposed techniques in the above mentioned paper, in the more realistic and applied case of current fields. The authors used different information source of the current field to solve the uncertainty.

The rapidly exploring random tree (RRT) technique [9] has been used by Rao and Williams [16] for determining energy-optimal paths that account for the influence of ocean currents-from model predictions. They also compared the result of RRT methods to grid-based methods, and offer an improvement in terms of avoiding high-energy shallow regions.

In contrast to the previous works, the proposed method offers an execution plan that can minimise navigational error for a dead reckoning vehicle and subsequently reduce the overall time for path execution. There have been recent advances in persistent monitoring [17], [18] that adapts the frequency of visits to each region based on the time scale on which that region changes. These studies were adapted for developing planning missions for underwater gliders [3], and are sensitive to the relative importance of different regions, while being naturally amenable to the unique constraints of the autonomous underwater glider. Here, we are motivated by these works, and extend this research by accounting for the variation in both current magnitude and direction, with respect to time, to reach a specific target point using a Gaussian model

and a modified MDP technique.

### III. MISSION PLANNING FRAMEWORK

In this work, we utilise predictions from an ocean model and a Markov Decision Process (MDP) to determine the best execution of a given path for better navigation accuracy, and minimal mission time, for an AUV in the presence of a current field distribution.

The motion-planning problem is to select the actions that minimise risk of drift-from-goal and minimise the time to goal. This problem is thus naturally posed as a Markov Decision Process ( $S; A; P; R$ ), where:  $S$  denotes the set of possible states of the AUV;  $A$  is the set of actions available from each state;  $P$  presents the transition probabilities  $P_a(s_i; s_j)$  where ( $s_i$ ) is the current state and ( $s_j$ ) is the possible next states under action ( $a$ );  $R$  defines the expected immediate reward for each transition and each action ( $a$ ).

1) *Ocean Model*: In this work, we utilise the Regional Ocean Modeling System (ROMS), which is run at the Jet Propulsion Laboratory (JPL), California Institute of Technology. This model is a split-explicit, free-surface, topography-following coordinate oceanic model. The model output has three nested horizontal resolutions covering the U.S. west coastal ocean (15 km), the southern California coastal ocean (5 km), and the SCB (2.2 km). The three nested ROMS domains are coupled online and run at the same time, exchanging boundary conditions at every time step of the coarser resolution domain. ROMS provides hindcasts, nowcasts, and hourly forecasts (up to 72 h) for the (SCB) [19]. The operational model assimilates temperature and salinity data from AUV, sea surface temperature from satellites, and surface currents from the high-frequency radar network. Detailed information on ROMS can be found in [20] and [21].

2) *MDP Mission Planning Algorithm*: A Markov decision process (MDP) is a mathematical framework for sequential decision making problems in stochastic domains. An MDP thus provides underlying semantics for the task of planning under uncertainty.

There are a number of algorithms to calculate the optimal policy in an MDP. Linear programming, value iteration, and policy iteration are the most commonly used. The computation of value function is a key factor in all three algorithms.

A value function can be defined as a value for each state  $S$  in the state space, with unambiguous representation of value functions as a vector of values for the different states. The solution algorithms can be implemented as a series of simple algebraic steps. Once the optimal value function  $V^*$  is computed, the optimal policy  $\pi^*$  is simply the greedy policy with respect to  $V^*$ .

Given two waypoints (Starting location and Target location) compute a path that minimises travel time by exploiting an uncertain, time-varying current field for an AUV. This problem can be naturally posed as MDP where the parameters of MDP are defined as follows:

*Possible states (S)*: the number of possible states will be equal to the number of cells in the discretized grid. The

Cartesian coordinates of the state of the AUV at the centre of a cell will be denoted by  $S_{i,j} = x_{i,j}, y_{i,j}, \psi_{i,j}$  where  $x_{i,j}, y_{i,j}, \psi_{i,j}$  denote x position, y position and heading angle for the AUV at  $cell_{i,j}$  respectively. An important assumption is that the horizontal velocity of the AUV is constant and equal to ( $V_{Glider}$ ).

*Actions available from each state (A)*: we assume that the AUV can move in eight directions,  $A = N, NE, E, SE, S, SW, W, NW$  as shown in Fig. 3.

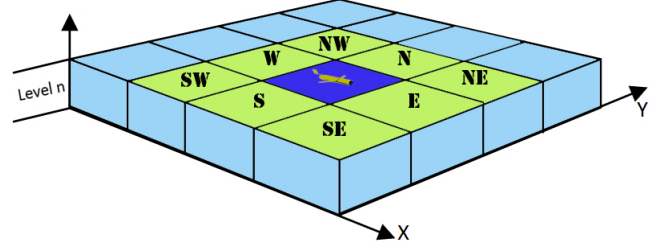


Fig. 3. A graphical representation of the eight possible end locations for the eight given actions of the AUV originating from the dark blue state and ending at the yellow state.

*Transition probabilities (P)*: The transition probabilities  $P : P_{s,a}(s, \hat{s})$  manage the probabilities of what state  $\hat{s}$  is entered after executing each action  $A$  from state  $s$ . In this work we find an innovative method based on Gaussian distribution to assign a realistic transition probabilities  $P_{s,a}$  in time varying current field to fit in the MDP framework.

To determine the transition probabilities  $P : P_{s,a}(s, \hat{s})$  the vector of the AUV velocity and current velocity at  $cell_{i,j}$  are added. The summation result of the two vectors represented by the magnitude  $\vec{F}$  and direction  $\omega$  using Eq. (1) - Eq. (3).

$$F_x = V_{min} \cos(\psi_{i,j}) + W_{i,j} \cos(\theta_{i,j}), \quad (1)$$

$$F_y = V_{min} \sin(\psi_{i,j}) + W_{i,j} \sin(\theta_{i,j}), \quad \text{and} \quad (2)$$

$$\vec{F} = \sqrt{F_x^2 + F_y^2}, \quad \omega = \tan^{-1}\left(\frac{F_y}{F_x}\right). \quad (3)$$

Figure 4 shows the normal distribution of transition probabilities ( $P$ ) by setting  $\omega$  from Eq. (3) as the mean value of a Gaussian distribution with standard deviation  $\sigma_\omega$  in each cell. The standard deviation will be selected by the user and is constant. The transition probabilities ( $P$ ) will be presented by the area governed by the intersection between the curve and the range angle (Green line) for each state.

*Reward for each transition and each action (R)*: The reward function is equal to two components. First, the direct reward value which will be calculated based on the current component facing the target cell, Fig. 5. The ratio between the current component facing the target point ( $W_{i,j} \cos(\theta_{i,j} + \theta_T)$ ) and the maximum expected current ( $W_{max}$ ) value will be calculated and multiplied by the weight ( $C1$ ) as shown in Eq. (4).

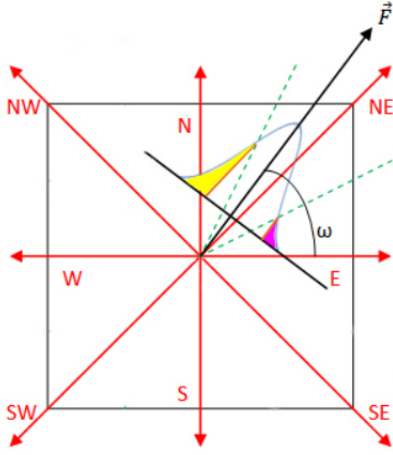


Fig. 4. The normal distribution of transition probabilities ( $P$ ) by setting  $\omega$  from Eq. (3) as the mean value of a Gaussian distribution with standard deviation  $\sigma_\omega$  in each cell. In this example, the total summation vector of the AUV velocity and current velocity represented by the black arrow, the probability to reach the North state given by the yellow area, the probability to reach the North-East state given by uncoloured area, and the probability to reach the East state given by the purple area.

$$R1_a(s_{i,j}) = \left( \frac{W_{i,j} \cos(\theta_{i,j} + \theta_T)}{W_{max}} \right) C1. \quad (4)$$

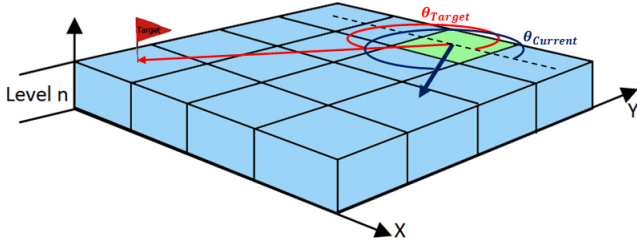


Fig. 5. Reward function. Where  $\theta_{Target}$  is the angle from each cell to the target cell,  $\theta_{current}$  is the current direction in each cell, and the red flagged cell is the target cell

The second component Fig. 6 will be equal to the absolute value of the difference between the heading angle and the actual angle, the actual angle is the resultant angle of combining the speed of the AUV and the current in the cell, divided by the heading angle and multiply the result by a weight ( $C2$ ) using Eq. (5).

$$R2_a(s_{i,j}) = \left| \frac{\theta_{heading_{i,j}} - \theta_{actual_{i,j}}}{\theta_{heading_{i,j}}} \right| C2. \quad (5)$$

Thus the reward function will be equal to

$$R_a(s_{i,j}) = R1_a(s_{i,j}) - R2_a(s_{i,j}). \quad (6)$$

It is important to note that the values of  $C1$  and  $C2$  can greatly effect the output of the algorithm. These weighting factors act as normalisation constants that scale the relative magnitudes of  $R1$  and  $R2$ , upon which the MDP is based. Even though  $R1$  and  $R2$  are both dimensionless quantities, they must be

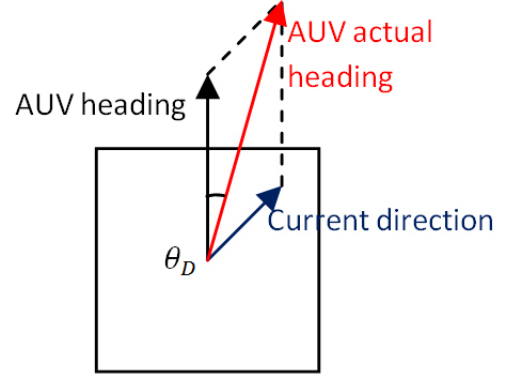


Fig. 6. Risk function. Where  $\theta_D$  represent the drift angle caused by the current in the cell. The black arrow shows the direction of AUV, blue arrow shows the direction of current, and red arrow shows the resultant heading angle of the AUV

properly scaled to incorporate their relative importance in the planning process. A larger  $C1$  value provides more emphasis on ocean currents, while a larger  $C2$  value emphasises heading direction. Figure 7 shows an example of the effect of  $C1$  and  $C2$ . Figure (7-a) shows an example of ocean current distribution, Fig. (7-b) shows the output of the algorithm when ignoring the value  $R2_a(s_{i,j})$ , i.e., ( $C2 = 0$ ). Figure (7-c) shows the output of the algorithm when  $C2 = C1$ , and Fig. (7-d) shows the output of the algorithm when ( $C2 = 10C1$ ).

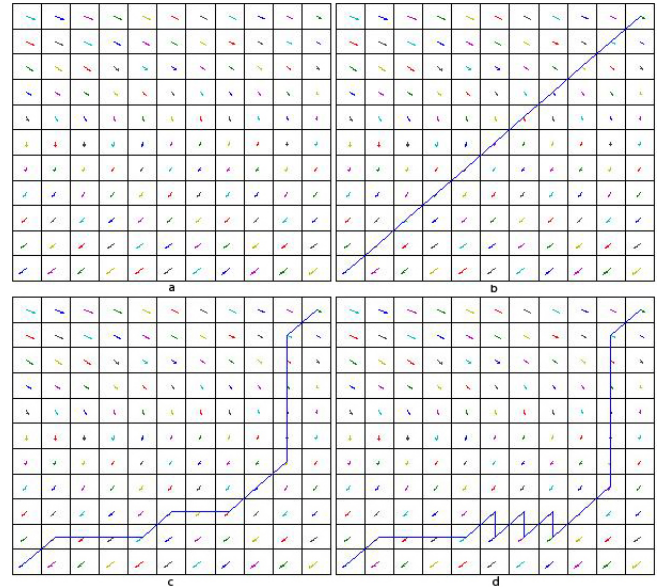


Fig. 7. Example of the effect of  $C1$  and  $C2$ , where (a) shows an example of ocean current distribution, (b) shows the output of the algorithm when ignoring the value  $R2_a(s_{i,j})$ , ( $C2 = 0$ ), (c) shows the output of the algorithm when  $C2 = C1$ , and (d) shows the output of the algorithm when ( $C2 = 10C1$ ).

Having defined the parameters of MDP, we can compute the value function ( $V(s)$ ) for a cell.

$$V(s_{i,j}) := E[R_a(s_{i,j}) + \gamma \sum (P_{s,a}(s, \delta) V(\delta))]. \quad (7)$$

The optimal value function ( $V^*(s)$ ) for a cell will be given by

$$V(s_{i,j}) := \max_a E[R_a(s_{i,j}) + \gamma \sum (P_{s,a}(s, \dot{s}) V(\dot{s}))], \quad (8)$$

where  $s$  is the initial state,  $\dot{s}$  the next possible state,  $R_a(s_{i,j})$  is the possible reward in state  $s_{i,j}$  taken an action  $a$ ,  $P_{s,a}(s, \dot{s})$  is the probability of reaching  $\dot{s}$  while applying action  $a$  in state  $s_{i,j}$ , and  $V(\dot{s})$  is the value function for state  $\dot{s}$ . It is important to notice that applying the previous equation without using the discount factor  $\gamma$  may lead to the AUV not reaching the goal because the reward function is totally dependent on the harvested power. Thus the factor  $\gamma$  that represents the time ratio ( $1 > \gamma > 0$ ) is added to the equation.

Identifying the optimal values  $V^*(s)$  will lead to determine the optimal policy  $\pi^*(s)$  using

$$\pi^*(s) = \arg \max_a (R_a(s_{i,j}) + \gamma \sum_{\dot{s} \in S} (P_{s,a}(s, \dot{s}) V^*(\dot{s})), \quad (9)$$

following the optimal policy will lead to the optimal path.

#### IV. PROBLEM SETUP AND VEHICLE DESCRIPTION

We propose to utilise transit regions through regions of less scientific importance (exploiting a specific layer of current) as a more accurate and time efficient method than always executing a standard sampling mission (performing full-depth profiles) over the same transect. Here, we assume that sampling in these regions is not restricted to be performed in a certain manner. Thus, we allow the vehicle to choose where in the water column to execute a particular portion of the path. The vehicle considered is a Slocum autonomous underwater glider, and the mission motivation is described in Section I-A.

##### A. Autonomous Underwater Gliders

As seen in Fig. 8, a Webb Slocum autonomous underwater glider is the vehicle for this study. Such a vehicle collects samples from the ocean for long-term ( $\sim 1$  month). A Slocum glider is torpedo-shaped vehicle that is a 1.5 m (length) by 21.3 cm (diameter). These vehicles are driven entirely by a variable buoyancy system to *fly* through the water. The vehicles forward velocity converted from the buoyancy-dependent vertical motion by the wings. Inflection points occur at depths and altitudes set in the user-defined mission plan. Moreover, by dead-reckoning the glider navigates with a sequence of dives and climbs, which forms a pattern that resemble a vertical sawtooth, between waypoints. Gliders are applied for their deployment endurance, because they provide an optimal way with minimal energy cost to obtain high-resolution spatial and temporal data. For similar reasons, on-board decision making and computation are generally not performed, and a priori planning techniques like the proposed method can greatly assist in mission execution for these vehicles.

Given their persistence, the data gathered by gliders are important for understanding physical forcing components acting on a regional scale and determining long-term variability. For such applications, to accurately rebuild and localize the data that are gathered for proper assessment by ocean scientists, we



Fig. 8. A Slocum glider preparing to start a mission.

require advanced techniques in persistent monitoring. Methods to increase navigational accuracy of autonomous gliders by using the prediction of ocean model have been previously studied by the authors, see [4], [5]. The need for increasing the repeatability and reconstructability of executed glider paths, has motivated further research in high-level planning methods.

##### B. Problem Setup

To demonstrate and validate the proposed methodology we conducted a proof-of-concept field experiment to examine a proxy transit region within the SCB. We selected two waypoints (W1, W2), see Fig. 9, that described a proxy transit region. The two way points are separated by 3.5 km. As the difference from a typical mission and our method is precisely in the transit regions, we examine the difference between traversing the segment using a standard mission scenario versus our proposed transit segment method. First, the vehicle started from point W1 aiming to point W2 using the proposed method. The vehicle surfaced when it reached W2. The vehicle then headed back to W1 using the proposed method. We note that there was no correction in position upon surfacing at W2, as seen in Fig. 10. Once the glider surfaces, it has achieved target point W1, and the second mission begins. After the initial execution, the glider executes another trip back and forth executing a standard method of Slocum glider operation all the way, see [5] for details on standard glider missions. We chose to start with our proposed method because it depends on synchronisation with the ocean model in time.

The ocean model divides the region of interest into four levels as shown in Table II, each level will be discretised into cubes of size of 2.2 km x 2.2 km x 20 – 30 m in depth Fig. 11.

For our planning methods, a 2.2 km x 2.2 km discretised grid is too coarse. Thus we used bilinear interpolation to reduce the grid resolution to 800 m.



Fig. 9. Search area for field test (green shaded) and predetermined 3.5 Km path between the chosen waypoints (W1,W2).

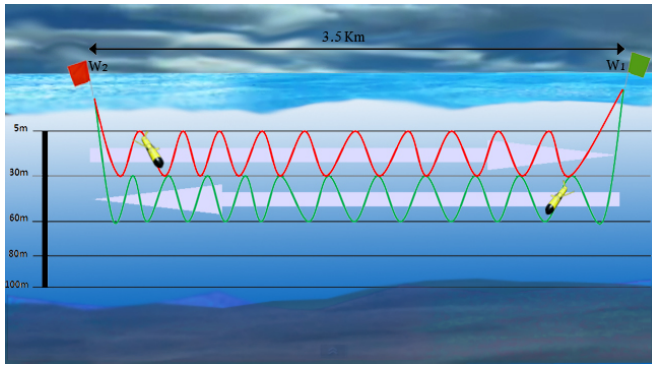


Fig. 10. Example of a possible solution for the case test shown in section IV-B. Where the depth vary between 5 m to 100 m, W1 and W2 are the chosen waypoints.

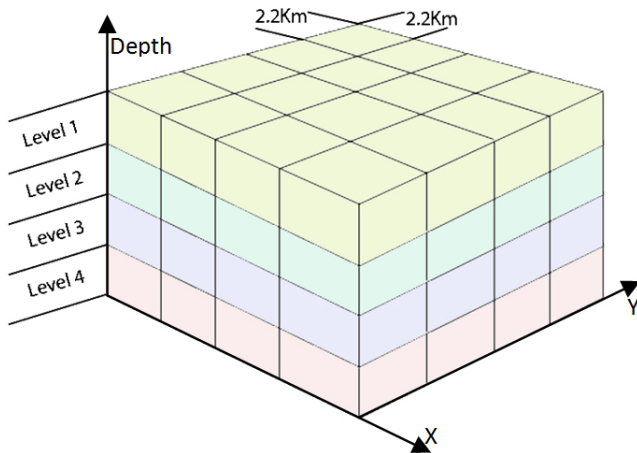


Fig. 11. Discretisation of the ocean model into levels and current cubes. Where the cube dimensions are 2.2 Km x 2.2 Km x Level depth.

TABLE II  
LEVEL DEPTH AND THICKNESS FOR THE TEST CASE SHOWN IN SECTION IV-B.

Level	Depth (m)	Level thickness (m)
Level 1	5 to 30	25
Level 2	30 to 60	30
Level 3	60 to 80	20
Level 4	80 to 100	20

## V. SIMULATIONS AND RESULTS

The paths are planned by incorporating ocean model predictions into a Markov Decision Process framework. This method incorporates the uncertainty of ocean currents and enables paths to be planned based on science-driven constraints and expert input. Here, sampling areas are defined as areas of higher importance within a mission domain. Transit areas are regions where the density of data collection required is less than within the sampling areas, or regions where the sampling objectives of the mission can be relaxed to offer more flexibility in path execution. In the sampling segments, the vehicle executes a standard sampling plan as defined by the ocean expert. In the transit segments, the mission planning model finds the best level strip within which to dive based on the magnitude and direction given by the ocean model for the specific area.

Here, we present both simulation predictions and field trials for an experiment conducted in the SCB. As the modification of our method specifically affects transit regions, the proof-of-concept experiment presented here examines a single transit region. We apply our algorithm to determine which level is best to dive through while the path is fixed. We compare the experimental results with the simulation predictions. In the following section, we represent the simulation for our field trial operating between 0800 GMT on 20 August, 2012 and 0000 GMT on 21 August 2012. The mission was actually executed between 1212 on 20 August 2012 and 0054 GMT on 21 August 2012. Due to delay in glider transit time to the designated experiment regions this time offset occurred.

### A. Simulations

We divided the mission into two parts; the transect from W1 to W2 ( $T_{12}$ ) and the transect from W2 to W1 ( $T_{21}$ ), as shown in Fig. 9. In this mission the proposed algorithm determined within which level to dive, with the level ranges given in Table II. To do this, two main concepts must be determined. First, which level has the favourable current to help the glider reaching the target with minimum drift and time. Second, which level has the minimum current variation with respect to depth and time.

Figure 12-A through 12-D shows the distribution of the ocean current in the test region for the four levels (1, 2, 3, 4), respectively and the vehicle behaviour. The black arrows indicate the current direction and the coloured arrows show the vehicle behaviour while incorporating the effect of the

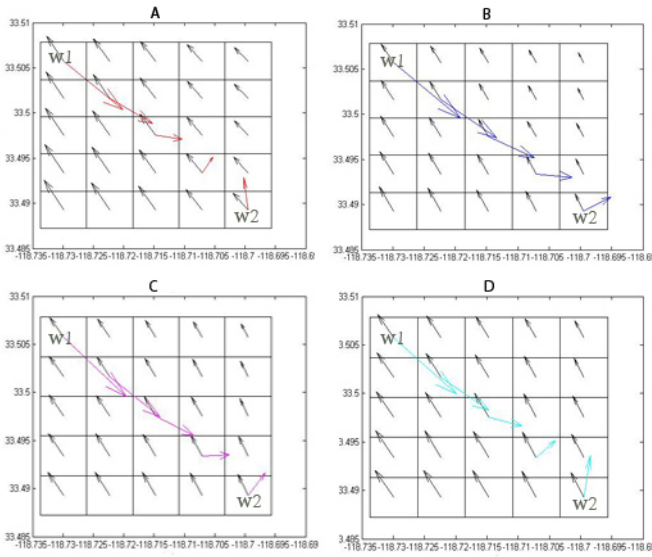


Fig. 12. The distribution of the ocean current in the test region for the four levels (1, 2, 3, 4) respectively and the vehicle behaviour while moving from W1 to W2 between  $t = 12$  and  $t = 16$ . Where the black arrows indicate the current direction and the coloured arrows show the resultant direction of the vehicle.

current magnitude and direction in each cell. From Fig 12 it can be seen that Level 2 is the best level to dive through since the final drift from the target is minimum. Figure 13 shows

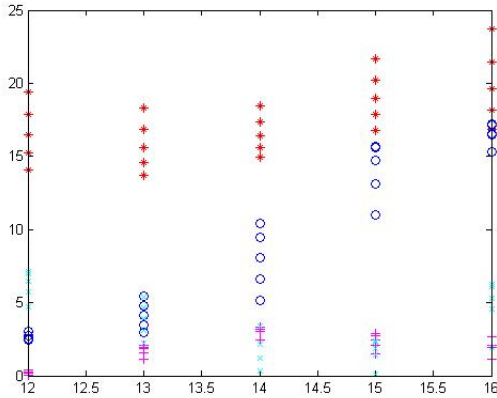


Fig. 13. Plot of standard deviation for the current direction in each cell from  $t = 12$  to  $t = 16$  (the actual operation time for the field trial). The red plot indicates Level 1, blue indicates Level 2, magenta indicates Level 3, and cyan indicates Level 4.

the plot of standard deviation for the current in each cell from  $t = 12$  to  $t = 16$  (the actual operation time for the field trial). The red plot indicates Level 1, blue indicates Level 2, magenta indicates Level 3, and cyan indicates Level 4. It can be seen that Level 3 has the least variability in current. However, the variation of current in Level 2, and 4 are also relatively small. An additional factor is the mean value of the current along the prescribed path. From Table III we can see that Level 2 has the minimum value for time. Combining this result with

TABLE III  
AVERAGE CURRENT MAGNITUDE ALONG THE TRACK BETWEEN  $t = 12$  AND  $t = 16$  ( $T_{12}$  OPERATION).

Level	mean value (m/s)
Level 1	0.1775
Level 2	0.1274
Level 3	0.1440
Level 4	0.1703

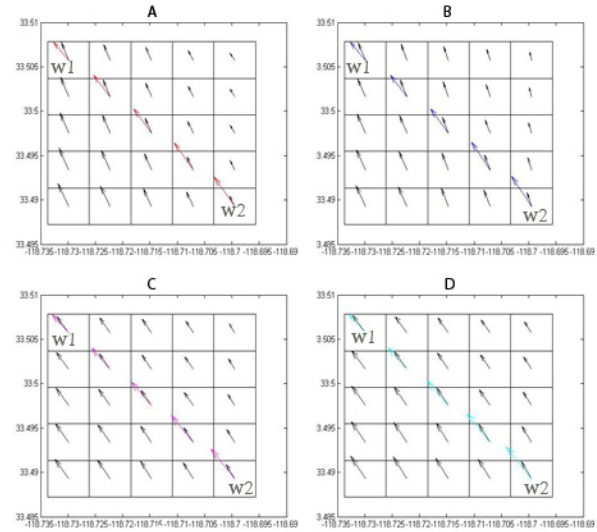


Fig. 14. The distribution of the ocean current in the test region for the four levels (1, 2, 3, 4), respectively and the vehicle behaviour for  $T_{21}$  between  $t = 16$  and  $t = 19$ . The black arrows indicate the current direction and the coloured arrows show the resultant direction of the vehicle.

previous result from Fig. 12 and Fig. 13 we can conclude that Level 2 is the best level to dive through for  $T_{12}$ . In this part of the mission, the offset in time did not effect the decision of the algorithm.

Figure 14-A through 14-D shows the ocean current distribution for the four levels (1, 2, 3, 4), respectively and the vehicle behaviour for  $T_{21}$ . The black arrows indicate the current direction and the coloured arrows show the vehicle behaviour while incorporating the effect of the current magnitude and direction in each cell. It can be seen there is not much difference between them, since the current direction is nearly the same as the vehicle direction. However, Level 3, and Level 4 provide the best results. The second factor which will effect the algorithm decision is the current variability within the same level. Figure 15 shows the plot of standard deviation for the current in each cell from  $t = 16$  to  $t = 19$  (the actual operation time for  $T_{21}$ ). The red plot indicates Level 1, blue indicates Level 2, magenta indicates Level 3, and cyan indicates Level 4. It can be seen that Level 3 and Level 4 provide better results, given out constraints. Table IV indicates that Level 4 has the best current magnitude, thus we can conclude Level 4 is the best level to dive through for  $T_{21}$ . This result is different than

the result we sent to the glider, and this because of the time offset experienced during the actual experiment. The level that the glider dove through was Level 1, since the calculations were based on travelling a few hours earlier than actually occurred.

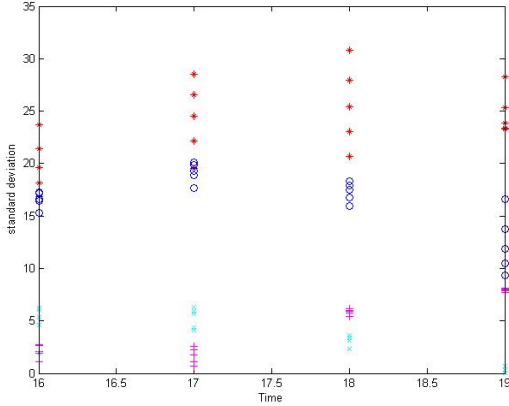


Fig. 15. Plot of the standard deviation for the current direction in each cell from  $t = 16$  to  $t = 19$  (the actual operation time for  $T_{21}$ ). The red plot indicates Level 1, blue indicates Level 2, magenta indicates Level 3, and cyan indicates Level 4.

TABLE IV  
AVERAGE CURRENT MAGNITUDE ALONG THE TRACK BETWEEN  $t = 16$   
AND  $t = 19$  ( $T_{21}$  OPERATION).

Level	mean value (m/s)
Level 1	0.1011
Level 2	0.1033
Level 3	0.1263
Level 4	0.1451

### B. Field Experiments

In this section, we will show the result of the field experiment and compare it with the simulation predictions. There were two factors that affected the results. The first factor was the offset in the starting time, as indicated previously. The second factor was the actual starting position of the mission differed from the proposed location by 1.18 km. This affected not only the distance to travel, but also the angle between the starting location and the goal waypoint for each section of the mission.

Figure 16 shows the result of the field test (red line), the simulation test (blue line) and the expected trajectory (green line). The operation started physically at the start point aiming to W2. The vehicle travelled for 4.4 km and surfaced at the point S1. The trip took 4 hours with average velocity 1.1 Km/h. The surface point S1 is 1.8 km from W2. This error would be smaller if the operation started from W1, based on our algorithm, the shift would have been less than 0.8 km as indicated by the green dot in Fig. 16.

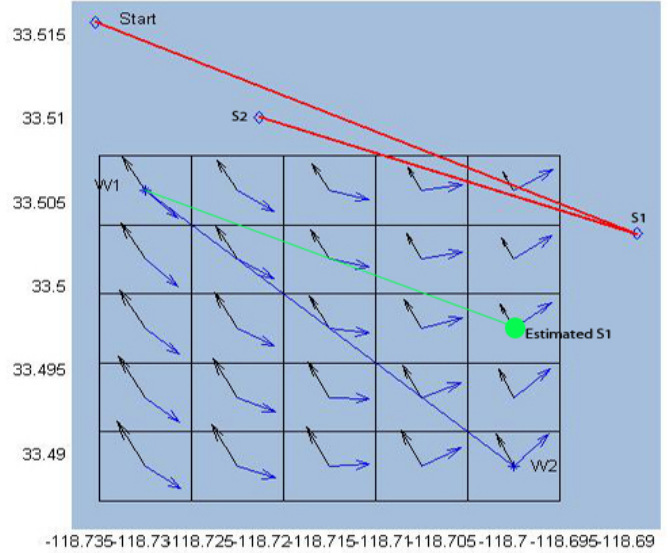


Fig. 16. The result of the operation  $T_{12}$  field test. Where Start is the actual starting point, S1 is the surface point while aiming W2. The red line is the actual trajectory using the algorithm, the green line is the expected trajectory, the blue line the proposed track, the black arrows is current direction between  $t = 12$  to  $t = 16$ , and the blue arrows are the vehicle behaviour at each cell.

Now we will Compare this result with the normal operation test. When the vehicle reached S2 we applied the standard mission scenario (diving through 5 m to 80 m) to reach W2 Fig. 17. The magenta line shows the real trajectory of the vehicle moving from S2 (Start2) to W2. The vehicle travelled 2.6 km and surfaced at point End1 which was 0.7 km away from W2. This experimental result was better than the predicted algorithm result. The vehicle went from (Start1 to End1) the current magnitude was 0.1212 m/s while when the vehicle went from (Start2 to End2) the current magnitude was 0.0758 which means when we operated our algorithm the current magnitude was 60% more than when operated the standard mission scenario. The travelled distance also gave the advantage for the proposed algorithm since it was 47% more than the distance travelled when we applied the standard mission scenario. Finally, the average speed of the vehicle while it was travelling from (Start2 to End2) was 0.9 Km/h which less than the average speed when it was travelling from (Start1 to End1).

The result of the field experiment based on the simulations for  $T_{21}$  can be seen in Fig. 18. The operation started from S1 aiming W2. The surface point was S2 which was 1.0 km away from the target point W1. The total distance travelled was 3.0 km with average velocity 0.9 km.

Even though the Level where the vehicle dove through while using the proposed algorithm was not the optimal for the actual conditions, the comparison with the field test gives good results. Figure 19 shows the trajectory line for the field test using our algorithm (Start1 End1) in red, the trajectory using the standard mission scenario (Start2 End2) in magenta, and the expected trajectory in green. Using the proposed algorithm



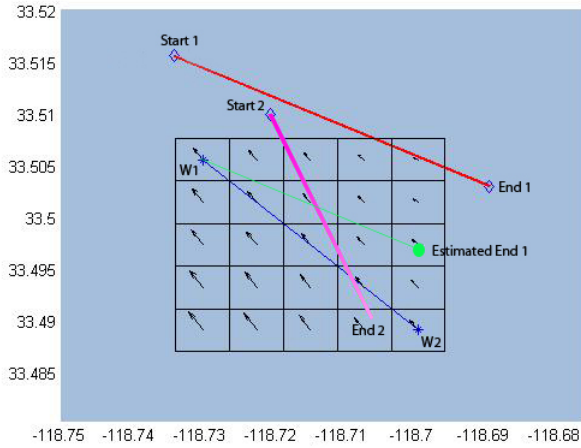


Fig. 17. The comparison between the W1 W2 using the standard mission scenario and W1 W2 using the proposed method. Start1 is the actual starting point while using the proposed algorithm, End1 is the actual surfacing point while using proposed algorithm, Start2 is the actual starting point while using the standard mission scenario, and End2 is the actual surfacing point while using normal operation. The red line is the actual trajectory using the algorithm, the green line is the expected trajectory, the blue line the proposed track, the black arrows is the current direction during  $T_{12}$  for the standard mission scenario between  $t = 19$  to  $t = 21$ .

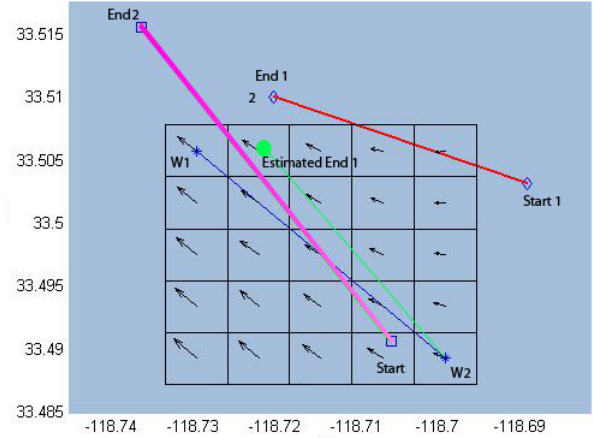


Fig. 19. The comparison for  $T_{21}$  using the standard mission scenario and  $T_{21}$  using our proposed method. Start1 is the actual starting point while using proposed algorithm, End1 is the actual surfacing point while using proposed algorithm. Start2 is the actual starting point while using normal operation, End2 is the actual surfacing point while using normal operation, red line is the actual trajectory using our algorithm. The green line is the expected trajectory, the blue line the proposed track, the black arrows are the current direction during operation  $T_{21}$  for the standard mission scenario between  $t = 21$  to  $t = 24$ .

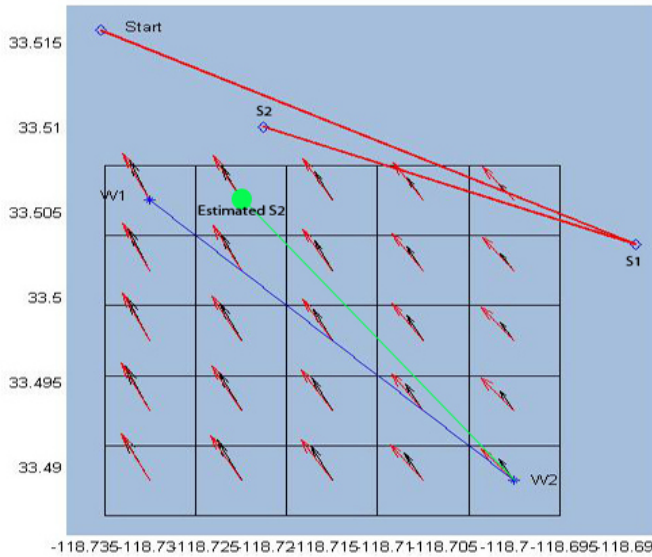


Fig. 18. The result of the execution of  $T_{21}$ . S1 is the actual starting point, S2 is the surface point while aiming W1. The red line is the actual trajectory using the algorithm, the green line is the expected trajectory, the blue line the proposed track, the black arrows is current direction between  $t = 12$  to  $t = 16$ , and the red arrows are the vehicle behaviour at each cell.

the vehicle surfaced 1 km away from the target point W1 while it surfaced 1.3 km away from target point W1 using normal operation. In addition, the direction of the current was helping the vehicle while operating in the standard mission scenario, and was partially against the vehicle while using our proposed algorithm.

## VI. CONCLUSIONS AND FUTURE WORK

This work presents a robust methodology for incorporating time-varying currents into a Markov Decision Process for path planning for underwater gliders. Combining the hybrid Gaussian distribution of ocean currents and the modified Markov Decision Process technique allowed the integration of uncertainty into a deterministic ocean model. A novel component of this method is that we enable the user (for example ocean expert) to designate a mission execution time, and the distinct partitioning, but rely on no a priori knowledge of the underlying science to compute the mission. This incorporates the experience of the expert without specifically writing out complex cost functions and optimization parameters.

Increasing navigational accuracy and extending deployment time via energy reduction is encoded into our method through the path computation. These advantages are demonstrated by through field trials comparing the proposed method to standard execution techniques. The results of the simulation compared to the experiments shows a better navigation accuracy and time-to-goal values. However, a better result could be obtained if we conduct the experiment operating two vehicles simultaneously; one with our proposed algorithm and the other executing the standard mission scenario.

The presented work is an initial investigation and experiment into the use of our proposed methodology. We plan to apply the techniques and algorithms to the motivating application presented in section I-A. Further field trials are planned for early 2013.

#### A. Acknowledgements

The authors would like to thank the USC CINAPS team [6] for the use of a Slocum glider to collect the data presented in this paper. We would also like to acknowledge the efforts of Arvind Pereira, Matthew Ragan and Carl Oberg for their valuable assistance with glider deployment and managing general operations.

This work was supported in part by the Early Career Academic Recruitment and Development (ECARD) Program of the Queensland University of Technology.

The ROMS predictions used were computed by the Jet Propulsion Laboratory (JPL), California Institute of Technology, under a contract with the National Aeronautics and Space Administration (NASA).

#### REFERENCES

- [1] O. Schofield, J. Kohut, D. Aragon, E. Creed, J. Graver, C. Haldman, J. Kerfoot, H. Roarty, C. Jones, D. Webb, and S. Glenn, "Slocum gliders: Robust and ready," *Journal of Field Robotics*, vol. 24, no. 6, pp. 473–485, 2007.
- [2] T. Dickey, Ed., *Ocean Sensing and Monitoring*, vol. 7317, 2009.
- [3] R. N. Smith, M. Schwager, S. L. Smith, B. H. Jones, D. Rus, and G. S. Sukhatme, "Persistent ocean monitoring with underwater gliders: Adapting sampling resolution," *Journal of Field Robotics*, vol. 28, no. 5, pp. 714 – 741, September/October 2011.
- [4] R. N. Smith, J. Kelly, Y. Chao, B. H. Jones, and G. S. Sukhatme, "Towards improvement of autonomous glider navigation accuracy through the use of regional ocean models," in *Proceedings of the 29th International Conference on Offshore Mechanics and Arctic Engineering*, Shanghai, China, June 2010, pp. 597–606.
- [5] R. N. Smith, J. Kelly, and G. S. Sukhatme, "Towards improving mission execution for autonomous gliders with an ocean model and kalman filter," in *Proceedings of the IEEE International Conference on Robotics and Automation*, Minneapolis, MN, May 2012, accepted, to appear.
- [6] R. N. Smith, J. Das, H. Heidarsson, A. Pereira, I. Cetinić, L. Darjany, M. Ève Garneau, M. D. Howard, C. Oberg, M. Ragan, A. Schnetzer, E. Seubert, E. C. Smith, B. A. Stauffer, G. Toro-Farmer, D. A. Caron, B. H. Jones, and G. S. Sukhatme, "USC CINAPS builds bridges: Observing and monitoring the Southern California Bight," *IEEE Robotics and Automation Magazine, Special Issue on Marine Robotics Systems*, vol. 17, no. 1, pp. 20–30, March 2010.
- [7] W. Zhang, T. Inane, S. Ober-Blobaum, and J. Marsden, "Optimal trajectory generation for a glider in time-varying 2d ocean flows b-spline model," in *Robotics and Automation, 2008. ICRA 2008. IEEE International Conference on*, may 2008, pp. 1083 –1088.
- [8] N. K. Yilmaz, C. Evangelinos, P. F. J. Lermusiaux, and N. M. Patrikalakis, "Path planning of autonomous underwater vehicles for adaptive sampling using mixed integer linear programming," *IEEE Journal of Oceanic Engineering*, vol. 33, no. 4, pp. 522 – 537, October 2008.
- [9] S. M. LaValle, "Rapidly exploring random trees: A new tool for path planning," Iowa State University, Tech. Rep., 1998.
- [10] K. Carroll, S. McClaran, E. Nelson, D. Barnett, D. Friesen, and G. William, "Auv path planning: an a\* approach to path planning with consideration of variable vehicle speeds and multiple, overlapping, time-dependent exclusion zones," in *Autonomous Underwater Vehicle Technology, 1992. AUV '92., Proceedings of the 1992 Symposium on*, jun 1992, pp. 79 –84.
- [11] P. Hart, N. Nilsson, and B. Raphael, "A formal basis for the heuristic determination of minimum cost paths," *Systems Science and Cybernetics, IEEE Transactions on*, vol. 4, no. 2, pp. 100 –107, july 1968.
- [12] A. Alvarez and A. Caiti, "Interactions of autonomous underwater vehicles with variable scale ocean structures," in *Proceedings of the IFAC World Conference Systems*, 2002.
- [13] A. Alvarez, A. Caiti, and R. Onken, "Evolutionary path planning for autonomous underwater vehicles in a variable ocean," *Oceanic Engineering, IEEE Journal of*, vol. 29, no. 2, pp. 418 – 429, april 2004.
- [14] B. Garau, A. Alvarez, and G. Oliver, "Path planning of autonomous underwater vehicles in current fields with complex spatial variability: an a\* approach," in *Robotics and Automation, 2005. ICRA 2005. Proceedings of the 2005 IEEE International Conference on*, april 2005, pp. 194 – 198.
- [15] B. Garau, M. Bonet, A. Alvarez, S. Ruiz, and A. Pascual, "Path planning for autonomous underwater vehicles in realistic oceanic current fields: Application to gliders in the western mediterranean sea," *Journal of Maritime Research*, vol. 6, pp. 5–22, 2009.
- [16] D. Rao and S. B. Williams, "Large-scale path planning for underwater gliders in ocean currents," in *Australasian Conference on Robotics and Automation*, 2009.
- [17] S. L. Smith and D. Rus, "Multi-robot monitoring in dynamic environments with guaranteed currency of observations," in *IEEE Conference on Decision and Control*, Atlanta, GA, Dec. 2010, pp. 514–521.
- [18] S. L. Smith, M. Schwager, and D. Rus, "Persistent robotic tasks: Monitoring and sweeping in changing environments," *IEEE Transactions on Robotics*, vol. 28, no. 2, p. 410, 2012.
- [19] Z. Li, Y. Chao, J. C. McWilliams, and K. Ide, "A three-dimensional variational data assimilation scheme for the regional ocean modeling system," *Journal of Atmospheric and Oceanic Technology*, vol. 25, p. 2074 – 2090, 2008.
- [20] A. F. Shchepetkin and J. C. McWilliams, "The regional oceanic modeling system (ROMS): a split-explicit, free-surface, topography-following-coordinate oceanic model," *Ocean Modelling*, vol. 9, pp. 347–404, 2005.
- [21] A. Shchepetkin and J. McWilliams, "Quasi-monotone advection schemes based on explicit locally adaptive dissipation," *Monthly Weather Review*, vol. 126, pp. 1541–1580, 1998.